Mechanical sensors

Multiphase Flow Analysis Using Piezoelectric Leaf-Cell Sensor Array

Dwight Swett* and Christopher Powell**

Aramco Research Center, Houston, TX 77084 USA
**Senior Member, IEEE*
***Member, IEEE*

Manuscript received 30 August 2022; accepted 14 September 2022. Date of publication 27 September 2022; date of current version 11 October 2022.

Abstract—The composition of the multiphase flow rates from hydrocarbon reservoirs has direct impact on the programs to optimize hydrocarbon production and for the identification of problems with production. However, the accurate measurement of the flow rates of oil, brine, and gas in three-phase regimes remains an intractable problem for current state-of-the-art sensor technologies. Here, we describe a piezoelectric acoustic leaf-cell sensor array providing an in situ real-time measurement of the distribution in three-phase flow fluid density over the wellbore cross section. The sensor array measurements are evaluated from experimental three-phase flow loop test data under a range of flow regimes comprised of 0–95% gas volume fraction and water/liquid volume ratio between 0 and 100%. The experimental data include three-phase flow transitions well into the nonlinear subsonic gas velocity region predicted by the Wood equation and show an average absolute error in three-phase fluid density prediction less than 0.05 g/cc over the entire test regimen.

Index Terms—Mechanical sensors, sensor applications, fluid composition analysis, Helmholtz resonator, piezoelectric resonator, multiphase volume fractions.

I. INTRODUCTION

The measurement of the multiphase flow rates of gas, oil, and brine production from hydrocarbon reservoirs is important for the hydrocarbon production optimization and timely detection of production problems. Reservoir and production engineers rely upon data that describe the volumetric and phase behavior of produced wellbore fluids moving from the geologic formation, through production tubing and surface equipment, and eventually into pipelines, in order to determine the time and method of extraction necessary to optimize the recovery of the hydrocarbons and thereupon the cost and potential profit margin that may be realized from the reservoir. Considerable research has been conducted to develop sensors and algorithms that address the estimation of the volume fractions of constituent media in two phase fluids [1], [2], [3], [4] using acoustic methods. Several approaches based upon radioactive sensing technologies [5], [6], [7], [8] have been proposed to estimate the volume fractions in three-phase fluids, but there is a lack of research results for the determination of the components of three-phase fluids using nonradioactive methods, particularly in the presence of an exsolved gas phase. To determine the compositional volume fractions of these three-phase flow regimes, two fluid properties' measurements are required for a closed-form determination, assuming the a priori knowledge of the constituent phase fluid properties.

In conventional systems, these two fluid properties' measurements are obtained using a combination of different sensor technologies deployed in consort at different locations in the flow stream. The sensor suites can be based upon optical, electrical, microwave, X-ray, and γ-ray radiation, as well as acoustic sensor physics approaches to estimate the two bulk fluid properties. Owing to concerns over risks posed to human health, technologies associated with microwave, X-ray, and γ-ray radiation are being reduced in their application, while other technologies, such as optical, dielectric, and ultrasonic,

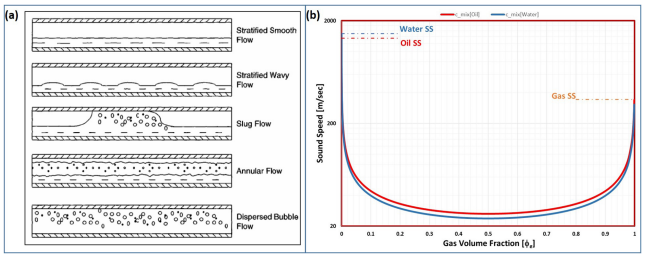

Fig. 1. Multiphase flow characteristics. (a) Horizontal flow regimes developed with multiphase fluids. (b) Influence of gas fraction on bulk fluid sound speed. Blue curve corresponds to single-phase water and red curve is single-phase oil, as both are injected with gas fraction.

are experiencing more developmental interest. Electrical resistance and capacitance probes are widely deployed for these multiphase flow analyses, but suffer from the effects of the inversion zone coinciding with the transition from water-to-oil liquid phases and within which both the technologies become insensitive to the composite liquid electrical properties. ypically, this inversion zone occurs in flows with liquid volume fractions for water and oil above 35%. The presence of an exsolved gas phase only complicates the problem. Electrical probes, for instance, do not distinguish between the electrical properties of oil and gas. Other sensor technologies, such as optical probes, have been incorporated as a means to broaden the conditions over which estimates for oil–water holdups can be made.

In a previous work [10], the development of a sensor providing simultaneous and congruent measurement of fluid density and sound speed was described for downhole multiphase compositional analysis involving gas saturated two-phase fluids. For multiphase flow metering at conditions that are well below the bubble point pressure for the multiphase fluid, such as conventional surface flow loop test conditions, the flow regime will involve the oil and brine phases as well as a third phase of exsolved gas as exemplified in the depictions of some classical horizontal multiphase flow regimes in Fig. 1(a). The presence of the exsolved gas phase violates the conditions of the calibration for sound

Corresponding author: Dwight Swett (e-mail: dwight.swett@aramcoamericas.com).
Associate Editor: I. Papautsky.
Digital Object Identifier 10.1109/LSENS.2022.3209587

speed described previously by Swett [10] for multiphase liquids and will require a different type of calibration incorporating additional parameters sensitive to gas volume fraction (GVF). For downhole conditions that typically remain well above the bubble point pressure, this is unnecessary. This is apparent from the Wood equation [12] for bulk compressibility, described as follows:

$$\rho = \phi_w \rho_w + \phi_o \rho_o + \phi_g \rho_g \tag{1}$$

$$\frac{1}{\rho c^2} = \frac{\phi_w}{K_w} + \frac{\phi_o}{K_o} + \frac{\phi_g}{K_g} \tag{2}$$

$$1 = \phi_w + \phi_o + \phi_g \tag{3}$$

where ϕ_w, ϕ_o, and ϕ_g are the volume fractions, ρ_w, ρ_o, and ρ_g are the mass densities, and K_w, K_o, and K_g are the bulk moduli of the water, oil, and gas phases, respectively, with ρ and c being the measured density and sound speed of the multiphase fluid, respectively. This system of three equations is linear in the three unknown phase volume fractions ϕ_w, ϕ_o, and ϕ_g, assuming that the fluid properties for the constituent phases are known a priori. For a two-phase liquid regime, only the density equation (1) and the volume fraction equation (3) are needed to determine the constituent liquid volume fractions, with intuitively simple trends resulting with effective bulk fluid properties residing between those of the two liquid phases. Conversely, the introduction of a small fraction of a third phase of exsolved gas introduces more significant nonlinearities, as illustrated in the sound speed versus gas phase fraction plot of Fig. 1(b) based upon the solution of (1)–(3) for single liquid phases of water and oil injected with fractions of gas. The plot in Fig. 1(b) illustrates that as small as 1% GVF injected into either a single-phase liquid of water or oil decreases the bulk fluid sound speed by more than an order of magnitude, which can be much less than the sound speed of the gas phase. This phenomenon develops due to the fact that the gas phase has negligible effect on the bulk fluid density, while its compressibility, being more than four orders of magnitude greater than either liquid phase, dominates the bulk compressibility of the three-phase fluid. This fundamental physical characteristic constitutes the problem confronting an accurate determination of the compositional properties of three-phase flow regimes holding exsolved gas fractions. Consequently, for conventional flow loop test conditions involving pressure well below the bubble point, an auxiliary fluid property measurement is required to substitute for the resonator sound speed measurement shown previously [10] until an extended methodology is determined, which encompasses conditions below the bubble point pressure. In the interim, an auxiliary sensor measurement is required, and for this series of tests, a commercial Coriolis water-cut meter measurement is used. The measurement approach and results are summarized for a set of multiphase fluid samples reaching bulk fluid sound speeds deep into the subsonic gas sound speed region. The accuracy of the sensor array measurements for real-time bulk fluid density and three-phase volume fractions is summarized for a range of flow loop test regimes ranging from 0 to 95% GVF and water cuts (water/liquid volume ratio) ranging between 0 and 100%.

II. LEAF-CELL SENSOR ARRAY

The sensor array is built upon a piezoelectric resonator that develops simultaneous and congruent measurement of bulk fluid mass density and sound speed in multiphase liquids. The simultaneity and the congruence of the acoustical properties measurements are derived from coupling between the piezoelectric resonator and the dilatational

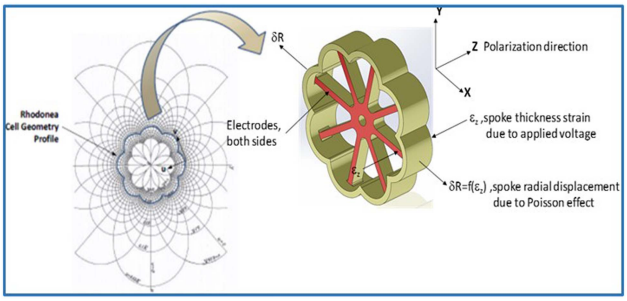

Fig. 2. Resonator geometry based on conformal mapping contours.

resonance of the fluid volume. This is formed intrinsically by the curvilinear contours of the leaf-cell-type piezoelectric structure acting to compress and extend the volume of fluid that flows through the cell structure creating an intrinsic Helmholtz cavity response based upon simply the closed contour leaf cell and the fluid volume. The vibrational characteristics of the leaf-cell "tines" are the basis for the piezo-structural-acoustic coupling that is created between the interior fluid and the spoke member electrodes of the resonator. The leaf-cell resonator is formed from the manipulation of the contour segments of the canonical Rhodonea conformal mapping geometry defined by the following relations [9]:

$$x = \pm\frac{1}{\sigma}\sqrt{\sigma + u}, \quad y = \pm\frac{1}{\sigma}\sqrt{\sigma - u}, \quad \sigma = \sqrt{u^2 + v^2} \tag{4}$$

where (u, v) are the Rhodonea conformal curvilinear coordinates, as illustrated in the constant coordinate (x, y) plot of Fig. 2. The conformal contour segments form an eightfold symmetry in the leaf-cell resonator geometry joined by eight central spoke members plated to function as the electrodes for electrical drive and sense, as described in [10].

For the sensor array configuration, the basic resonator feedthrough assembly is integrated with a metal feedthrough housing, protective flowthrough shroud, and pressure feedthrough connector, as shown in Fig. 3(a) and (b). The flowthrough shroud design includes a pattern of radially directed openings sized sufficiently large to allow rapid fluid flow across the sensor resonator but sufficiently small to prevent impact damage to the resonator from large-diameter solid particles in the flow stream. To enhance the sensitivity of the leaf-cell sensor to fluid acoustic properties and improve the measurement for fluid density, an exterior metal Helmholtz cavity wall is integrated in the flowthrough shroud structure, as shown in Fig. 3(a) and (b), to couple the leaf-cell resonator intrinsic interior Helmholtz resonator effect with the leaf-cell external acoustic field. The addition of the exterior field-coupling Helmholtz cavity wall increases the acoustic pressure field internal and external of the piezoelectric leaf-cell resonator. The preferred design for the field-coupling Helmholtz shroud is a steel material that provides the proper acoustic impedance to promote the enhancement of the leaf-cell sensor measurement sensitivities. The sensor array is designed symmetric about the pipe centerlines and aligned parallel with the gravity vector, as shown in Fig. 3(c) and (d), for the optional five-sensor configuration. This placement of the sensors allows the characterization of the flow property distribution under stratified, annular, slug, and bubbly flows. The sensor array manifold was integrated into a horizontal leg of the commercial flow loop test facility, as shown in Fig. 4.

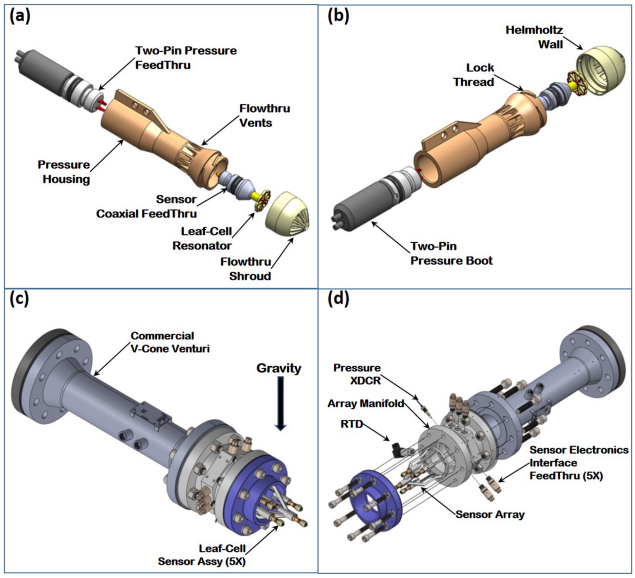

Fig. 3. Sensor array description. (a) and (b) Sensor assembly exploded views. (c) and (d) Sensor array assembly for flow loop tests.

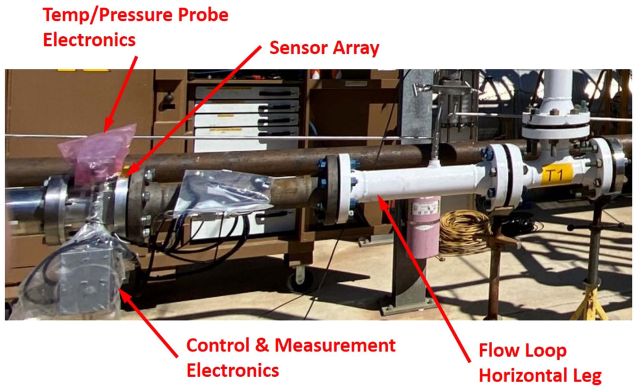

Fig. 4. Sensor array flow loop test setup, SwRI facility.

III. MULTIPHASE FLOW LOOP TESTS

A regimen of commercial flow loop tests was conducted at the Southwest Research Institute (SwRI), a P&FDD-approved facility, to characterize the performance of the sensor array multiphase flow metering technology under a wide range of flow conditions that included flow rates in the range of 2000–10000 barrels/day, gas fractions of 0–95%, water cuts of 0–100%, using an Exxsol D110 synthetic oil as the hydrocarbon, methane and nitrogen as two separate gas media, and two water salinities (4% and 13% by mass). Prior to the flow loop testing, each of the piezoelectric resonators in the sensor array was calibrated for fluid density measurement using a set of calibrated laboratory fluid samples and statistical regression techniques similarly as described in [10]. A set of five different calibrated single-phase fluid samples and air was tested to determine each of the sensor density measurement characteristics. The range of fluid density values in the calibration set varied from air at 0.001 g/cc to 1.14 g/cc for a water–salt brine. The resulting density measurement algorithm was determined to follow a simple quadratic relation in the frequency shift of the admittance phase spectra peak for the top and bottom sensors and a simple quadratic relation in the frequency shift of the admittance magnitude minima for the middle sensor in the array.

Theoretically, a density measurement can be combined with an auxiliary water-cut measurement to estimate the three-phase fluid volume fractions. For exsolved GVF, we first consider the system of equations in (1)–(3) and introduce a standard water-cut measurement $\omega = \phi_w/\phi_L$ as a known parameter obtained from an auxiliary sensor such as a commercial infrared or microwave device, which defines the ratio of water volume fraction to the total liquid fraction of the multiphase fluid. We can then rewrite the density equation as

$$\rho = (1-\phi_g)[(1-\omega)\rho_o + \omega\rho_w] + \phi_g\rho_g \tag{5}$$

and obtain for a prediction of GVF

$$\phi_g = \left[\frac{\omega\rho_w + (1-\omega)\rho_o - \rho\_\text{arr}}{\omega\rho_w + (1-\omega)\rho_o - \rho_g}\right] \tag{6}$$

where ρ_arr denotes an array leaf-cell sensor fluid density measurement. Predictions for oil and water fractions, ϕ_o_arr and ϕ_w_arr, are then determined using (5) and (6) as

$$\phi_o = \left[\frac{(1-\phi_g)\rho_w - (\rho\_\text{arr} - \rho_g\phi_g}{\rho_w - \rho_o}\right] \tag{7}$$

$$\phi_w = \left[\frac{(\rho\_\text{arr} - \rho_g\phi_g) - (1-\phi_g)\rho_o}{\rho_w - \rho_o}\right]. \tag{8}$$

Thus, the direct measurement of the multiphase fluid density ρ_arr from the sensor array in conjunction with the measurement of the water cut ω from an auxiliary device allows a real-time estimate for the component three-phase volume fractions in the liquid–gas flow.

A set of different flow regimes was measured in the SwRI multiphase flow loop in which the reference water cut ω was obtained from an inline commercial Coriolis meter located immediately after the brine–oil mixing point and prior to the gas injection point measured using an inline commercial mass airflow sensor. Two water–salt brine densities were 1.024 and 1.09 g/cc, and the oil density was 0.80 g/cc. The reference fluid volume fractions, composition phase fluid properties, and component and bulk flow rates were measured using a combination of Coriolis meters and gas mass flow rate sensors. The pressure and temperature along the flow loop test were measured using inline sensors. The sensor array predictions for the density of the multiphase bulk flow were calculated using a simple arithmetic average of the three leaf-cell sensors in the array. The results are summarized graphically in Fig. 5(a), and a representative excerpt of the data is tabulated in Fig. 5(b). The results in Fig. 5 show that the sensor array provides good predictions for multiphase fluid density over the wide range of flow regimes that were tested, with an average absolute error of less than 0.05 g/cc.

The transient response of predicted density from the array is shown for three test cases of GVF (10, 60, and 95%) in Fig. 6. The density measurements summarized in Fig. 6 for the range of GVF illustrate the sensitivity of the array resonators to transient flow effects. The results in Fig. 5 show the transients average out to give good density predictions over the range of flow conditions.

Estimates for three-phase volume fractions were calculated from the transient sensor array density measurement in combination with an auxiliary inline SwRI Coriolis water-cut measurement ω using the relations of (5)–(8). The results are summarized graphically in the plot of Fig. 7, with average errors of 6.3, 3.6, and 3.1% for gas, oil, and water volume fractions, respectively, relative to the SwRI facility calibrated volume fraction readings. The results in Fig. 7 indicate that

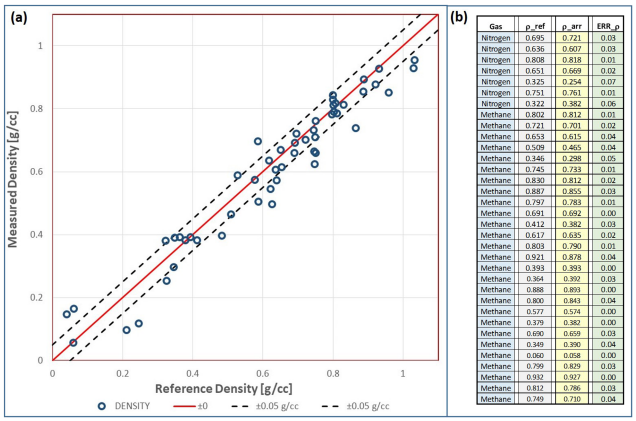

Gas	ρ_ref	ρ_arr	ERR_ρ
Nitrogen	0.695	0.721	0.03
Nitrogen	0.636	0.607	0.03
Nitrogen	0.808	0.818	0.01
Nitrogen	0.651	0.669	0.02
Nitrogen	0.325	0.254	0.07
Nitrogen	0.751	0.761	0.01
Nitrogen	0.322	0.382	0.06
Methane	0.802	0.812	0.01
Methane	0.721	0.701	0.02
Methane	0.653	0.615	0.04
Methane	0.509	0.465	0.04
Methane	0.346	0.298	0.05
Methane	0.745	0.733	0.01
Methane	0.830	0.812	0.02
Methane	0.887	0.855	0.03
Methane	0.797	0.783	0.01
Methane	0.691	0.692	0.00
Methane	0.412	0.382	0.03
Methane	0.617	0.635	0.02
Methane	0.803	0.790	0.01
Methane	0.921	0.878	0.04
Methane	0.393	0.393	0.00
Methane	0.364	0.392	0.03
Methane	0.888	0.893	0.00
Methane	0.800	0.843	0.04
Methane	0.577	0.574	0.00
Methane	0.379	0.382	0.00
Methane	0.690	0.659	0.03
Methane	0.349	0.390	0.04
Methane	0.060	0.058	0.00
Methane	0.799	0.829	0.03
Methane	0.932	0.927	0.00
Methane	0.812	0.786	0.03
Methane	0.749	0.710	0.04

Fig. 5. Observed versus predicted density, SwRI three-phase flow tests. (a) Graphical comparison. (b) Excerpt of representative data.

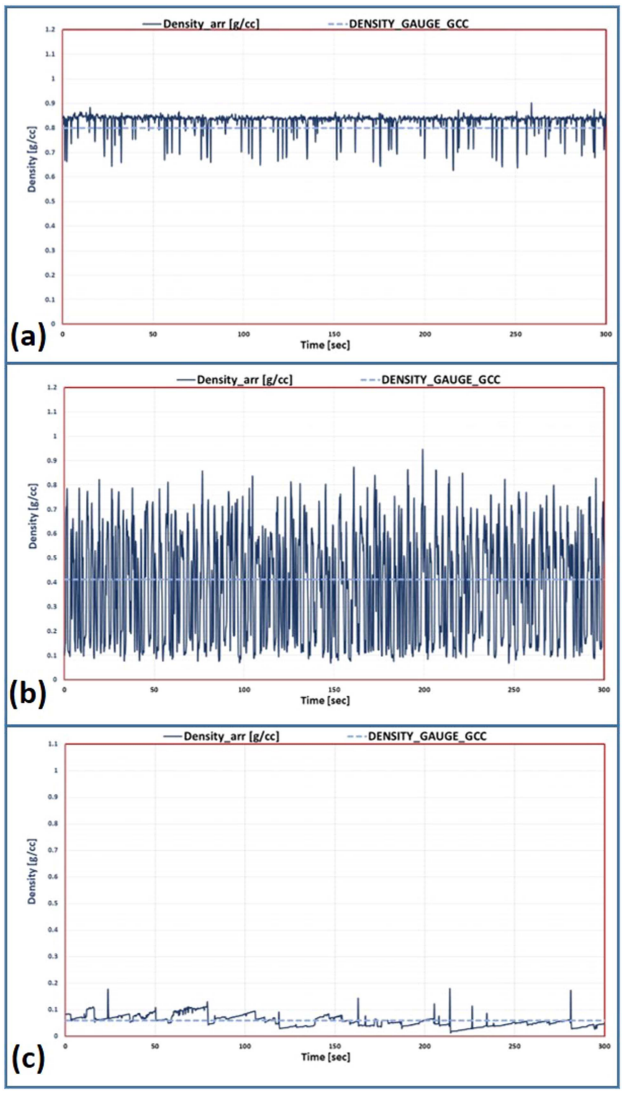

Fig. 6. Transient sensor array average density measurements and flow loop references, for three-phase flow GVF/OVF/WVF. (a) 0.10/0.63/0.27. (b) 0.61/0.07/0.32. (c) 0.95/0.0/0.05.

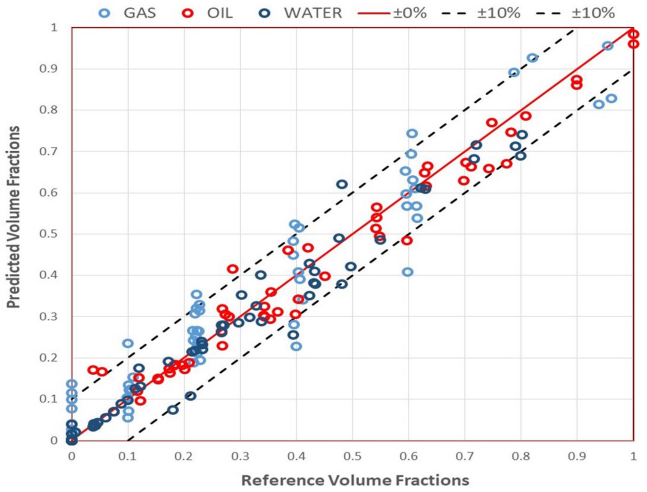

Fig. 7. Observed versus predicted three-phase volume fractions using a combination of sensor array density and Coriolis water-cut measurements.

the use of the sensor array density measurement in conjunction with an auxiliary water-cut measurement is a feasible approach for three-phase flow analysis.

REFERENCES

[1] A. Chaudhuri, C. F. Osterhoudt, and D. N. Sinha, "An algorithm for determining volume fractions in two-phase liquid flows by measuring sound speed," *J. Fluids Eng.*, vol. 134, no. 1, 2012, Art. no. 101301.

[2] G. Kuster and M. Toskoz, "Velocity and attenuation of seismic waves in two-phase media. Part I: Theoretical formulations," *Geophysics*, vol. 39, no. 5, pp. 587–606, 1974.

[3] G. Meng, J. Jaworski, and N. M. White, "Composition measurements of crude oil and process water emulsions using thick-film unltrasonic transducers," *Chem. Eng. Process.*, vol. 35, pp. 383–391, 2006.

[4] C. Tsouris and L. L. Tavlarides, "Volume fraction measurements of water in oil by an ultrasonic technique," *Ind. Eng. Chem. Res.*, vol. 32, pp. 998–1002, 1993.

[5] R. Ramos, L. E. B. Brandao, R. Schirru, C. M. Salgado, C. M. N. A. Pereira, and A. X. da Silva, "Volume fraction calculation in multiphase system such as oil-water-gas using neutron," in *Proc. Int. Nucl. Atlantic Conf.*, 2007.

[6] G. H. Roshani, A. Karami, E. Nazemi, and F. Shama, "Volume fraction determination of the annular three-phase flow of gas-oil-water using adaptive neuro-fuzzy inference system," *Comp. Appl. Math.*, vol. 37, pp. 4321–4341, 2018.

[7] A. R. Nejad, D. Naderi, and S. Setayeshi, "Improving the measurement of volume fraction of multiphase fluids based on attenuation of gamma rays without the use of artificial intelligence," *MAPAN J. Metrol. Soc. India*, vol. 36, pp. 869–874, 2021.

[8] C. M. Salgado, R. S. de Freitas Dam, C. de Carvalho Conti, and W. L. Salgado, "Three-phase flow meters based on X-rays and artificial neural network to measure the flow compositions," *Flow Meas. Instrum.*, vol. 82, 2021, Art. no. 102075.

[9] P. H. Moon and D. E. Spencer, *Field Theory Handbook*, 2nd ed. Berlin, Germany: Springer-Verlag, 1988.

[10] D. W. Swett, "Experimental characterization of a piezoelectric leaf-cell sensor for simultaneous fluid density and sound speed measurement," *IEEE Sens. Lett.*, vol. 4, no. 5, May 2020, Art. no. 4500404.

[11] R. Urick, "A sound velocity method for determining the compressibility of finely divided substances," *J. Appl. Phys.*, vol. 18, pp. 983–987, 1947.

[12] A. B. Wood, *A Textbook of Sound*. London, U.K.: G. Bell, 1930.